

Understanding and Exploring the Whole Set of Good Sparse Generalized Additive Models

Zhi Chen^{*1} Chudi Zhong^{*1} Margo Seltzer² Cynthia Rudin¹

Abstract

In real applications, interaction between machine learning model and domain experts is critical; however, the classical machine learning paradigm that usually produces only a single model does not facilitate such interaction. Approximating and exploring the Rashomon set, i.e., the set of all near-optimal models, addresses this practical challenge by providing the user with a searchable space containing a diverse set of models from which domain experts can choose. We present a technique to efficiently and accurately approximate the Rashomon set of sparse, generalized additive models (GAMs). We present algorithms to approximate the Rashomon set of GAMs with ellipsoids for fixed support sets and use these ellipsoids to approximate Rashomon sets for many different support sets. The approximated Rashomon set serves as a cornerstone to solve practical challenges such as (1) studying the variable importance for the model class; (2) finding models under user-specified constraints (monotonicity, direct editing); (3) investigating sudden changes in the shape functions. Experiments demonstrate the fidelity of the approximated Rashomon set and its effectiveness in solving practical challenges.

1. Introduction

A key ingredient for trust in machine learning models is *interpretability*; it is more difficult to trust a model whose computations we do not understand. However, building interpretable models is not easy; even if one creates a model that is sparse and monotonic in the right variables, it likely is still not what the domain expert is looking for. In fact, domain experts often cannot fully articulate the constraints

their problem requires. This leads to an often painful iterative process where a machine learning algorithm, which is typically designed to produce only one model, is now asked to produce another, and possibly many more after that. Hence, the classical machine learning paradigm is broken because it was not designed for *choice* among models. In other words, the classical machine learning paradigm was not designed for the situation in which domain experts would be able to see and understand a model, criticize it, and expect it to change instantly in a specific way.

Here, we work in a new paradigm where an *algorithm produces many models from which to choose*, instead of just one (Breiman, 2001; Xin et al., 2022; Semenova et al., 2022). Algorithms in this new paradigm produce or approximate the *Rashomon set* of a given function class. The Rashomon set is the set of models that are approximately as good as the best model in the class. That is, it is the set of all good models. Rashomon sets for many real problems are surprisingly large (D’Amour et al., 2020; Marx et al., 2020; Hsu & Calmon, 2022), and there are theoretical reasons why we expect large numbers of simple, good models to exist (Semenova et al., 2022). The question we ask here is how to explicitly find the Rashomon set for the class of *sparse generalized additive models* (sparse GAMs).

GAMs are one of the most widely used forms of interpretable, predictive models (Hastie & Tibshirani, 1990; Lou et al., 2013; Agarwal et al., 2021) and have been applied to complex problems such as medical records (Caruana et al., 2015; Lengerich et al., 2022), where they can provide the same accuracy as the best black box models. Sparse GAMs include the class of scoring systems, which are widely used in hospitals for almost every subfield of medicine (Kessler et al., 2005; Moreno et al., 2005; Six et al., 2008) and in criminal justice for a century (Burgess, 1928; Borden, 1928; Austin et al., 2010; Latessa et al., 2010). Thus, an important previously-missing piece of the Rashomon set paradigm is *how to obtain the Rashomon set of sparse GAMs*.

Because the Rashomon set of sparse GAMs is continuous and has no analytical form, we present methods to approximate it, knowing that it is convex for each support set. We first study how to approximate the Rashomon set with an ellipsoid for a fixed support set. Our gradient-based

^{*}Equal contribution ¹Department of Computer Science, Duke University, USA ²Department of Computer Science, University of British Columbia, Canada. Correspondence to: Zhi Chen <zhi.chen1@duke.edu>, Chudi Zhong <chudi.zhong@duke.edu>.

optimization algorithm is able to find the largest volume ellipsoid inscribed in the true Rashomon set. Leveraging the properties of ellipsoids, we can also efficiently approximate Rashomon sets of numerous support sets that are subsets of the original support set. We show experimentally in Section 5 that this approximation captures most of the Rashomon set while not including too many models outside of it.

Approximating the Rashomon set by ellipsoids enables us to solve many practical challenges of GAMs through efficient convex optimization. We first use our Rashomon set approximation to study the importance of variables among a set of well-performing models, called *variable importance range*. This is essentially the Model Class Reliance, which measures the variable importance of models in the Rashomon set (Fisher et al., 2019); previously, ranges of variance importance have been studied only for linear models (Fisher et al., 2019) and tree models (Xin et al., 2022; Smith et al., 2020). We also show how to efficiently use the ellipsoid approximation to search for near-optimal models with monotonicity constraints. The Rashomon set empowers users to be able to arbitrarily manipulate models. As users edit models, their edits are either already in the Rashomon set (which we can check easily) or they can easily be projected back into the Rashomon set using the technique in Section 4.4. Thus, being able to approximate the full Rashomon set for GAMs brings users entirely new functionality, going way beyond what one can do with just a set of diverse models (Danna et al., 2007; Ahanor et al., 2022; Hara & Maehara, 2017; Hara & Ishihata, 2018; Ruggieri, 2017; 2019; Kissel & Mentch, 2021). Also, the ability to sample GAMs efficiently from the approximated Rashomon set allows us to investigate whether the variations or sudden changes observed in a single model are indicative of true patterns in the dataset or simply random fluctuations.

Since our work provides the first method for constructing Rashomon sets for sparse GAMs, there is no direct prior work. There has been prior work on related problems, such as constructing Rashomon sets for decision trees (Xin et al., 2022), and the Rashomon sets for linear regression are simply described by ellipsoids (Semenova et al., 2022); Rashomon sets for linear regression models have been used for decision making (Tulabandhula & Rudin, 2014), robustness of estimation (Coker et al., 2021), and holistic understanding of variable importance (Fisher et al., 2019; Dong & Rudin, 2020; Xin et al., 2022). Our work will allow these types of studies to generalize to GAMs.

2. Background

A sample is denoted as (\mathbf{x}, y) , where \mathbf{x} is the p dimensional feature vector and y is the target. The j^{th} dimension of the feature vector is x_j . A generalized additive model (GAM)

(Hastie & Tibshirani, 1990) has the form

$$g(E[y]) = \omega_0 + f_1(x_1) + f_2(x_2) + \cdots + f_p(x_p) \quad (1)$$

where ω_0 is the intercept, f_j 's are the shape functions and g is the link function, e.g., the identity function for regression, or the logistic function for classification. Each shape function f_j operates only on one feature x_j , and thus the shape function can directly be plotted. This makes GAMs interpretable since the entire model can be visualized through 2D graphs. In practice, a continuous feature is usually divided into bins (Lou et al., 2013), thereby its shape function can be viewed as a step function, i.e.,

$$f_j(x_j) = \sum_{k=0}^{B_j-1} \omega_{j,k} \cdot \mathbf{1}[b_{j,k} < x_j \leq b_{j,k+1}], \quad (2)$$

where $\{b_{j,k}\}_{k=0}^{B_j}$ are the bin edges of feature j , leading to B_j total bins. This is a linear function on the binned dataset whose features are one-hot vectors. $\omega = \{\omega_{j,0}, \omega_{j,1}, \dots, \omega_{j,B_j-1}\}_{j=1}^p$ is the weight vector. For simplicity, we use this formulation in the rest of our paper.

Given a dataset $\mathcal{D} = \{(\mathbf{x}_i, y_i)\}_{i=1}^n$, we use the logistic loss $\mathcal{L}_c(\omega, \omega_0, \mathcal{D})$ as the classification loss. To regularize the shape function, we also consider a weighted ℓ_2 loss $\mathcal{L}_2(\omega)$ on the coefficients and total number of steps in the shape functions $\mathcal{L}_s(\omega)$ as penalties. Specifically,

$$\mathcal{L}_2(\omega) := \sum_{j=1}^p \sum_{k=0}^{B_j-1} \pi_{j,k} \omega_{j,k}^2,$$

where $\pi_{j,k} = \frac{1}{n} \sum_{i=1}^n \mathbf{1}[b_{j,k} < x_{ij} \leq b_{j,k+1}]$ is the proportion of samples in bin k of feature j . The weighted ℓ_2 term not only penalizes the magnitude of the shape function, but also implicitly *centers* the shape function by setting the population mean to 0: any other offsets would lead to suboptimal $\mathcal{L}_2(\omega)$. This is inspired by Lou et al. (2013), which explicitly sets the population mean to 0. To make the shape functions fluctuate less, we penalize the total number of steps in all shape functions, i.e.,

$$\mathcal{L}_s(\omega) = \sum_{j=1}^p \sum_{k=0}^{B_j-1} \mathbf{1}[w_{j,k} \neq w_{j,k+1}],$$

which is similar to the ℓ_0 penalty of Liu et al. (2022). Combining classification loss and penalty yields the total loss:

$$\mathcal{L}(\omega, \omega_0, \mathcal{D}) = \mathcal{L}_c(\omega, \omega_0, \mathcal{D}) + \lambda_2 \mathcal{L}_2(\omega) + \lambda_s \mathcal{L}_s(\omega). \quad (3)$$

Following the definition of Semanova et al. (2022), we define the Rashomon set of sparse GAMs as follows:

Definition 2.1. (θ -Rashomon set) For a binned dataset \mathcal{D} with n samples and m binary features, where $\omega \in \mathbb{R}^m$ defines a generalized additive model. The θ -Rashomon set is a set of all $\omega \in \mathbb{R}^m$ with $\mathcal{L}(\omega, \omega_0, \mathcal{D})$ at most θ :

$$R(\theta, \mathcal{D}) := \{\omega \in \mathbb{R}^m, \omega_0 \in \mathbb{R} : \mathcal{L}(\omega, \omega_0, \mathcal{D}) \leq \theta\}. \quad (4)$$

Note that we use $\mathcal{L}(\omega, \omega_0)$ to represent $\mathcal{L}(\omega, \omega_0, \mathcal{D})$ and $R(\theta)$ to represent $R(\theta, \mathcal{D})$ when \mathcal{D} is clearly defined.

3. Approximating the Rashomon Set

3.1. GAM with Fixed Support Set (Method 1)

Suppose we merge all adjacent bins with the same ω_j . The set of bins after merging is called the support set. For a GAM with fixed support set, the \mathcal{L}_s term is fixed and the problem is equivalent to logistic regression with a weighted ℓ_2 penalty. For simplicity, in the remaining paper, ω also includes ω_0 . In this case, the loss $\mathcal{L}(\omega)$ is a convex function, and the Rashomon set $R(\theta)$ is a convex set. Hence, we propose to approximate $R(\theta)$ with an ellipsoid centered at ω_c . Specifically, the approximated Rashomon set is:

$$\hat{R} := \{\omega \in \mathbb{R}^m : (\omega - \omega_c)^T \mathbf{Q} (\omega - \omega_c) \leq 1\}, \quad (5)$$

where \mathbf{Q} and ω_c are the parameters defining the ellipsoid that we optimize given different θ s. We discuss our optimization method next.

Initialization: Since the support set is fixed, for now, we treat \mathcal{L}_s as a constant. A Taylor expansion on $\mathcal{L}(\omega)$ at the empirical risk minimizer ω^* yields:

$$\mathcal{L}(\omega) \approx \mathcal{L}(\omega^*) + \nabla \mathcal{L}^T (\omega - \omega^*) + \frac{1}{2} (\omega - \omega^*)^T \mathbf{H} (\omega - \omega^*) + O((\omega - \omega^*)^3).$$

Since ω^* is the empirical risk minimizer, the gradient $\nabla \mathcal{L} = 0$. If we ignore the higher order terms, we get a quadratic function, i.e., $\mathcal{L}(\omega) \approx \mathcal{L}(\omega^*) + \frac{1}{2} (\omega - \omega^*)^T \mathbf{H} (\omega - \omega^*)$. Plugging this quadratic function into the Rashomon set formula, we get exactly an ellipsoid, i.e.,

$$\frac{1}{2} (\omega - \omega^*)^T \mathbf{H} (\omega - \omega^*) \leq \theta - \mathcal{L}(\omega^*).$$

Given this approximation, we initialize ω_c with ω^* and \mathbf{Q} with $\mathbf{H}/(2(\theta - \mathcal{L}(\omega^*)))$.

Gradient-based optimization: The initialization might be imperfect in practice, because the gradient is assumed to be 0, and the higher order terms are completely ignored. Therefore, we propose to further optimize \mathbf{Q} and ω_c through gradient descent. We aim to maximize the volume of \hat{R} and guarantee that almost all points in \hat{R} are also in $R(\theta)$. Mathematically, the objective is

$$\min_{\mathbf{Q}, \omega_c} \det(\mathbf{Q})^{\frac{1}{2m}} + C \cdot \mathbb{E}_{\omega \sim \hat{R}(\mathbf{Q}, \omega_c)} [\max(\mathcal{L}(\omega) - \theta, 0)]. \quad (6)$$

The volume of \hat{R} is proportional to $\det(\mathbf{Q})^{-1/2}$, therefore we minimize $\det(\mathbf{Q})^{1/(2m)}$ in the objective. m is included in the exponent to normalize by the number of dimensions. In the second term of Eq (6), we draw samples from $\hat{R}(\mathbf{Q}, \omega_c)$ and penalize it if the sample is outside $R(\theta)$; C is a large constant to make sure this happens rarely. Note that we can use the reparameterization trick to convert the sample ω drawn from \hat{R} into a purely stochastic part and a deterministic part related to \mathbf{Q} and ω_c , and calculate the gradients accordingly. Details are shown in Appendix B.

3.2. GAMs with Different Support Sets (Method 2)

Method 1 can accurately approximate the Rashomon set given fixed support set. However, if we want the Rashomon set for many different support sets, applying Method 1 repeatedly can be time-consuming. In this subsection, we propose a blocking method, Method 2, to efficiently approximate the Rashomon sets with many smaller support sets after getting an approximated Rashomon set for a large support set by Method 1.

Approximating the Rashomon set with an ellipsoid can be helpful in approximating the Rashomon sets with smaller support sets. Specifically, if the bins of the smaller support set are generated by merging bins in the original support set, it is equivalent to forcing the coefficients of these merged bins to be the same. Formally, this is a hyperplane P in the solution space defined by a set of linear constraints

$$P := \{\omega \in \mathbb{R}^m : \omega_k = \omega_{k+1} = \dots = \omega_\kappa\}, \quad (7)$$

where the k^{th} to the κ^{th} bins in the original support set are merged to create a single bin in the new support set. The hyperplane's intersection with any ellipsoid, e.g., \hat{R} , is still an ellipsoid, which can be calculated analytically. Specifically, if we rewrite \mathbf{Q} in form of block matrices, i.e.,

$$\mathbf{Q} = \begin{bmatrix} \mathbf{Q}_{1:k-1, 1:k-1} & \mathbf{Q}_{1:k-1, k:\kappa} & \mathbf{Q}_{1:k-1, \kappa+1:m} \\ \mathbf{Q}_{1:k-1, k:\kappa}^T & \mathbf{Q}_{k:\kappa, k:\kappa} & \mathbf{Q}_{k:\kappa, \kappa+1:m}^T \\ \mathbf{Q}_{1:k-1, \kappa+1:m}^T & \mathbf{Q}_{\kappa+1:m, k:\kappa} & \mathbf{Q}_{\kappa+1:m, \kappa+1:m} \end{bmatrix},$$

we can obtain the quadratic matrix $\tilde{\mathbf{Q}}$ for the new support set by summing up the k^{th} to κ^{th} rows and columns, i.e.,

$$\tilde{\mathbf{Q}} = \begin{bmatrix} \mathbf{Q}_{1:k-1, 1:k-1} & \mathbf{q}_{1:k-1} & \mathbf{Q}_{1:k-1, \kappa+1:m} \\ \mathbf{q}_{1:k-1}^T & q_{mid} & \mathbf{q}_{\kappa+1:m}^T \\ \mathbf{Q}_{1:k-1, \kappa+1:m}^T & \mathbf{q}_{\kappa+1:m} & \mathbf{Q}_{\kappa+1:m, \kappa+1:m} \end{bmatrix},$$

where $q_{mid} = \sum_{i=k}^{\kappa} \sum_{j=k}^{\kappa} Q_{i,j}$, $\mathbf{q}_{1:k-1}$ and $\mathbf{q}_{\kappa+1:m}$ are two column vectors obtained by summing all columns of $\mathbf{Q}_{1:k-1, k:\kappa}$ and $\mathbf{Q}_{\kappa+1:m, k:\kappa}$. The linear term of the original support set is $\ell := \mathbf{Q} \omega_c$. Similarly, we can obtain the linear term of the new support set $\tilde{\ell}$ by summing up k^{th} to κ^{th} elements of the ℓ vector, i.e.,

$$\tilde{\ell} = [\ell_1, \dots, \ell_{k-1}, \sum_{i=k}^{\kappa} \ell_i, \ell_{\kappa+1}, \dots, \ell_m]^T.$$

With this, we can calculate the new center of ellipsoid, $\tilde{\omega}_c = \tilde{\mathbf{Q}}^{-1}\tilde{\ell}$, and the upper bound of the new ellipsoid $u = 1 - \omega_c^T \mathbf{Q} \omega_c + \tilde{\omega}_c^T \tilde{\mathbf{Q}} \tilde{\omega}_c$. This new ellipsoid $R_P := P \cap \hat{R}$, which satisfies both Equation 5 and 7, is defined as

$$R_P := \{\omega \in \mathbb{R}^m : (\omega - \tilde{\omega}_c)^T \tilde{\mathbf{Q}} (\omega - \tilde{\omega}_c) \leq u\},$$

where if $u \leq 0$, R_P is empty. If we want to merge multiple set of bins, the calculations can be slightly modified to summing up sets of rows and columns separately corresponding to the sets of bins to be merged. R_P serves as a simple approximation of the Rashomon set for the smaller support set. Every ω in R_P is also in the Rashomon set because it is a subset of the original ellipsoid \hat{R} , and all points in \hat{R} are in the Rashomon set. In fact, since the support set gets smaller, \mathcal{L}_s becomes smaller too, and the loss is even lower, i.e., for ω in R_P , $\mathcal{L}(\omega) \leq \theta - \lambda_0(\kappa - k)$.

Explore different support sets with size \tilde{K} : Using the blocking method mentioned above, we can approximate the Rashomon set for many different support sets that are the subsets of the original support set. The approximation of the ellipsoid for a smaller support set is more accurate when the size difference between the original support set and the new support set is smaller. Therefore, instead of using a very large support set at the beginning, we use a sparse GAM algorithm such as FastSparse (Liu et al., 2022) with a relatively weaker sparsity penalty to get a support set S whose size K is moderately larger than the size of support sets we want to explore, but covers all bins we want to potentially merge to form the new support set. For simplicity of defining the loss threshold of the Rashomon set, here we consider only support sets with size \tilde{K} . If we want to explore different \tilde{K} , we can repeat this process. Suppose our goal is to explore the Rashomon set with loss threshold δ . The first step is to use the methods in Section 3.1 to obtain the ellipsoid \hat{R} approximating the θ -Rashomon set on the original support set, where $\theta = \delta + \lambda_0(K - \tilde{K})$. Then we can enumerate all possible ways ($\binom{K-p}{K-\tilde{K}}$ ways in total) to merge bins in the original support set to get any subset \tilde{S} whose size is \tilde{K} , and calculate the intersection (i.e., ellipsoid) $R_{P_{\tilde{S}}} := P_{\tilde{S}} \cap \hat{R}$ between \hat{R} and the hyperplane $P_{\tilde{S}}$ corresponding to merging S into \tilde{S} . All nonempty $R_{P_{\tilde{S}}}$ are valid approximations of the Rashomon set.

4. Applications of the Rashomon Set

We now show four practical challenges related to GAMs that practitioners can now solve easily using the approximated Rashomon sets.

4.1. Variable Importance within the Model Class

Variable importance can be easily measured for GAMs. For example, Explainable Boosting Machines (Lou et al., 2013;

Nori et al., 2019) measures the importance of each variable by the weighted mean absolute coefficient value of bins corresponding to this variable, i.e.,

$$VI(\mathbf{x}_{:,j}) = \sum_{k=0}^{B_j-1} \pi_{j,k} |w_{j,k}|.$$

This measure is based on one model, but given the Rashomon set, we can now provide a more holistic view of how important a variable is by calculating the range of variable importance among many well-performing models; this is called the model class reliance (Fisher et al., 2019). Specifically, we can get VI_- and VI_+ as the lower and upper bounds of this range, respectively. For example, the range of importance of feature j is defined as

$$[VI_-(\mathbf{x}_{:,j}), VI_+(\mathbf{x}_{:,j})] = [\min_{\omega \in R(\theta)} VI(\mathbf{x}_{:,j}), \max_{\omega \in R(\theta)} VI(\mathbf{x}_{:,j})]. \quad (8)$$

A feature with a large VI_- is important in all well-performing models; a feature with a small VI_+ is unimportant to every well-performing model. We use \hat{R} to approximate $R(\theta)$ and estimate VI_- by solving a linear programming problem with a quadratic constraint, and we estimate VI_+ by solving a mixed-integer programming problem. Solving these problems also gives the user a model in the Rashomon set that relies the most (or the least) on a certain feature, which can be useful in many real applications.

Lower bound of variable importance: VI_- of feature j can be obtained by solving the following linear programming problem.

$$\begin{aligned} \min_{[\omega_{j,0}, \dots, \omega_{j,B_j-1}]} & \sum_{k=0}^{B_j-1} \pi_{j,k} |\omega_{j,k}| \\ \text{such that } & (\omega - \omega_c)^T \mathbf{Q} (\omega - \omega_c) \leq 1. \end{aligned} \quad (9)$$

Since $\pi_{j,k} \geq 0$, Problem (9) can be solved using an LP solver. The objective minimizes variable importance, and the constraint ensures the solution is in the Rashomon set.

Upper bound of variable importance: The maximization problem cannot be solved through linear programming since $[\omega_{j,0}, \dots, \omega_{j,B_j-1}]$ can be arbitrarily large. Instead, we formulate it as a mixed-integer program. Let M be a relatively large number (e.g., 200 is large enough for real applications) and let I_k be a binary variable.

$$\begin{aligned} \max_{[\omega'_{j,0}, \dots, \omega'_{j,B_j-1}]} & \sum_{k=0}^{B_j-1} \pi_{j,k} \omega'_{j,k} \\ \text{s.t. } & (\omega - \omega_c)^T \mathbf{Q} (\omega - \omega_c) \leq 1 \\ & \omega_{j,k} + M \times I_k \geq \omega'_{j,k}, \quad \forall k \in \{0, \dots, B_j - 1\} \\ & -\omega_{j,k} + M \times (1 - I_k) \geq \omega'_{j,k}, \quad \forall k \in \{0, \dots, B_j - 1\} \\ & \omega_{j,k} \leq \omega'_{j,k}, \quad -\omega_{j,k} \leq \omega'_{j,k}, \quad \forall k \in \{0, \dots, B_j - 1\}. \end{aligned} \quad (10)$$

The last two constraints ensure that $\omega'_{j,k}$ is defined as the absolute value of $\omega_{j,k}$. However, solving mixed-integer programs is usually time-consuming. We propose another way to solve the maximization problem. Since $\omega_{j,k}$ can be either positive or negative, we enumerate all positive-negative combinations for $\omega_{j,k}, k \in \{0, \dots, B_j - 1\}$ and solve the LP problem with the sign constraint enforced (see Algorithm 2 in the Appendix).

4.2. Monotonic Constraints

Another use-case for the GAM Rashomon set is finding an accurate model that satisfies monotonicity constraints. This can be obtained by solving a quadratic programming problem. For example, if a user wants $f_j(\mathbf{x}_j)$ to be monotonically increasing, the optimization problem can be formalized as:

$$\begin{aligned} \min_{\omega} & (\omega - \omega_c)^T \mathbf{Q} (\omega - \omega_c) \\ \text{s.t. } & \omega_{j,k} \leq \omega_{j,k+1}, k \in \{0, \dots, B_j - 1\}, \end{aligned} \quad (11)$$

where we check that the solution is ≤ 1 ; that is, whether the solution ω is in the approximated Rashomon set.

4.3. Changes in the shape functions

Sudden changes (e.g., a jump or a spike) in the shape functions of GAMs are known to be useful signals for knowledge discovery (Caruana et al., 2015; Lengerich et al., 2022) and debugging the dataset (Chen et al., 2021). However, due to the existence of many almost equally good models that have different shape functions, it is hard to identify if a change is a true pattern in the dataset or just a random artifact of model fitting. However, with the approximated Rashomon set, we can calculate the proportion of models that have such a change among all near-optimal models and visualize the shape functions (see Section 5.4).

4.4. Find the model within the Rashomon set closest to the shape function requested by users

As discussed, the main benefit of the Rashomon set is to provide users a choice between equally-good models. After seeing a GAM’s shape functions, the user might want to make edits directly, but their edits can produce a model outside of the Rashomon set. We thus provide a formulation that projects back into the Rashomon set, producing a model within the Rashomon set that follows the users’ preferences as closely as possible. We find this model by solving a quadratic programming problem with a quadratic constraint. Let ω_{req} be the coefficient vector that the user requests. The problem can be formulated as follows:

$$\min_{\omega} \|\omega - \omega_{req}\|_2^2 \text{ s.t. } (\omega - \omega_c)^T \mathbf{Q} (\omega - \omega_c) \leq 1. \quad (12)$$

Problem (12) can be easily solved through a quadratic programming solver.

5. Experiments

Our evaluation answers the following questions: 1. How does our method compare to baseline methods for approximating the Rashomon set? 2. How does the approximated Rashomon set help us understand the range of variable importance in real datasets? 3. How does the approximated Rashomon set deliver a model that satisfies users’ requirements? 4. How does the Rashomon set help us investigate changes in the shape function?

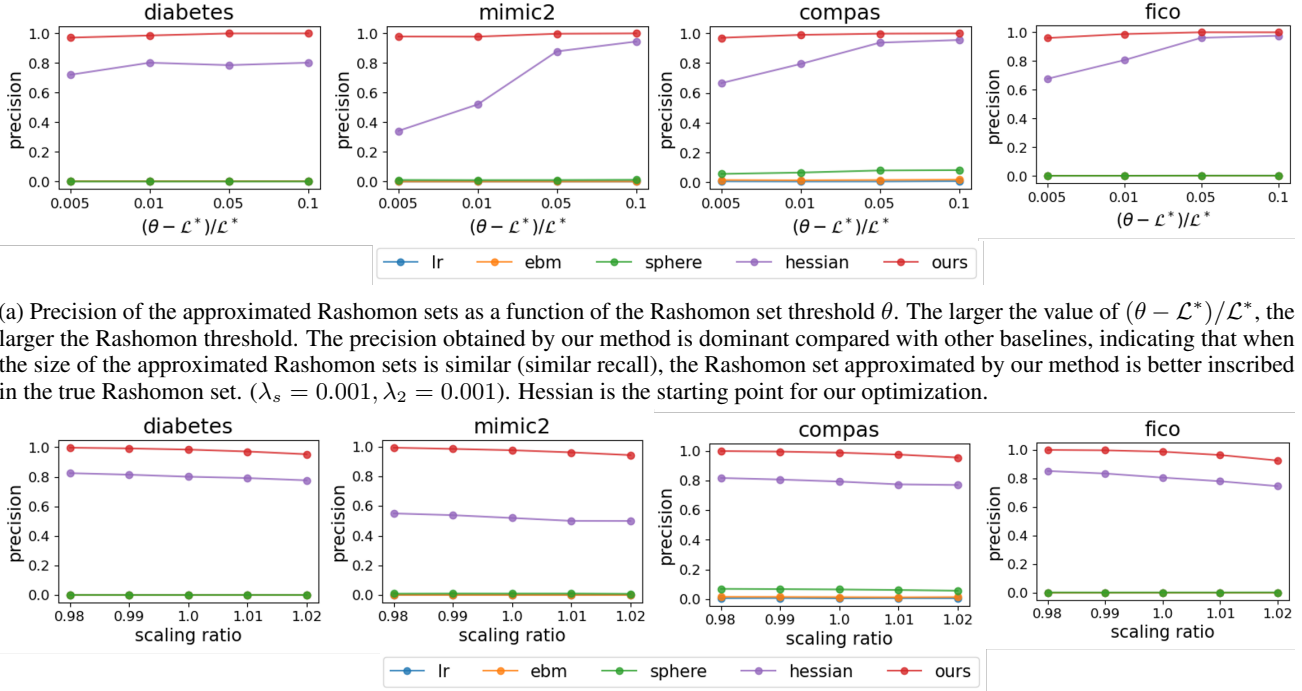
We use four datasets: a recidivism dataset (COMPAS) (Larson et al., 2016), the Fair Isaac (FICO) credit risk dataset (FICO et al., 2018), a Diabetes dataset (Smith et al., 1988), and an ICU dataset MIMIC-II (Saeed et al., 2002).

5.1. Precision and volume of the approximated Rashomon set

As we mentioned in Section 3, our goal is to create an approximation of the Rashomon set whose volume is as large as possible, while guaranteeing that most points in the approximated Rashomon set are within the true Rashomon set. To measure precision of our approximation, models within and outside the true Rashomon set $R(\theta)$ are considered as “positive” and “negative” respectively; models within and outside the approximated Rashomon set \hat{R} are considered as “predicted positive/negative.” Accordingly, the precision is defined as the proportion of points (ω, ω_0) , equally weighted and within \hat{R} , having $\mathcal{L}(\omega, \omega_0) \leq \theta$, i.e., they are in $R(\theta)$. The recall is defined as the proportion of points in $R(\theta)$ that are also in \hat{R} . Note that $\text{recall} = \frac{\text{Vol}(\hat{R} \cap R(\theta))}{\text{Vol}(R(\theta))} = \text{precision} \times \frac{\text{Vol}(\hat{R})}{\text{Vol}(R(\theta))}$. Since $\text{Vol}(R(\theta))$ is a constant, given the same volume $\text{Vol}(\hat{R})$, recall is proportional to precision.

To fairly compare with other methods, we first rescale the Rashomon set approximated by baselines to have the same volume as our \hat{R} . Then, we sample 10,000 points from our \hat{R} and rescaled baseline Rashomon sets, calculate their loss and estimate the precision.

One baseline is using the hessian initialization of \mathbf{Q} , i.e. $\mathbf{H}/(2(\theta - \mathcal{L}(\omega^*)))$, denoted as “hessian” in our comparison. Another baseline is to use the identity matrix to approximate \mathbf{Q} , i.e., the approximated set is a sphere. Another type of baseline comes from fitting GAMs on bootstrap sampled subsets of data. We thus get coefficient vectors from two different methods (logistic regression and EBMs, Lou et al. 2013, fitted on the same support set) on many subsets of data. This approach only samples a finite set of coefficient vectors rather than producing a closed infinite set such as an ellipsoid, and therefore its volume is not measurable. Thus, we use optimization to find the minimum volume ellipsoid that covers most coefficient vectors. This is the MVEE problem (Todd & Yildirim, 2007); more details are provided



(a) Precision of the approximated Rashomon sets as a function of the Rashomon set threshold θ . The larger the value of $(\theta - \mathcal{L}^*)/\mathcal{L}^*$, the larger the Rashomon threshold. The precision obtained by our method is dominant compared with other baselines, indicating that when the size of the approximated Rashomon sets is similar (similar recall), the Rashomon set approximated by our method is better inscribed in the true Rashomon set. ($\lambda_s = 0.001, \lambda_2 = 0.001$). Hessian is the starting point for our optimization.

(b) Tradeoff between precision and the size of the approximated Rashomon sets. Our method dominates baselines on all four datasets. As the scaling ratio increases, the precision starts to decrease. ($\lambda_s = 0.001, \lambda_2 = 0.001, \theta = 1.01\mathcal{L}^*$). Hessian is our starting point.

Figure 1. Precision versus the size of the approximated Rashomon set.

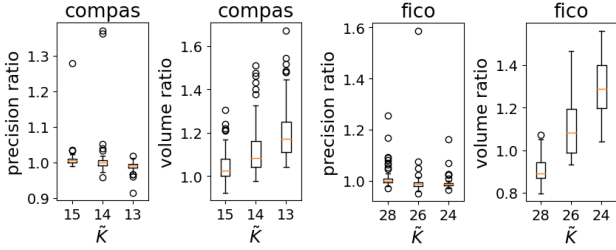


Figure 2. Box plots of the volume ratio and precision ratio of Method 1 over Method 2 across different \tilde{K} , for two datasets. It shows Method 2 performs similarly to Method 1.

in Appendix C. Sampling from the posterior distribution of a Bayesian model is also a way to get many different GAMs. We tried Bayesian logistic regression (using Hamiltonian Monte Carlo), but it is too slow (≥ 6 hours) to converge and produce enough samples to construct the minimum volume ellipsoid. So we did not include this baseline.

Figure 1 compares the precision and volume of our Rashomon set with baselines. Figure 1a shows our Rashomon set has dominant precision compared with baselines when the volume of the approximated Rashomon sets are the same. In other words, the Rashomon set approximated by our methods is the largest intersection with the true Rashomon set. The Rashomon set approximated by

the hessian is worse than ours but better than other baselines, which means our proposed initialization is already relatively better than approximating by a sphere and other baselines. Also, as θ becomes larger, the hessian method becomes better and sometimes close to the result after optimization. Logistic regression and EBM with bootstrapping do not achieve good precision. This is because coefficient vectors trained by these two methods on many subsets of data can be too similar to each other, leading to ellipsoids with defective shapes that do not match the true Rashomon set boundary even after rescaling.

In general, shrinking the approximated Rashomon set leads to higher precision and expanding it leads to better recall. Figure 1b shows the performance of different methods under this tradeoff. Our method still dominates others even when we rescaled the volume with different factors.

The previous experiments evaluate the performance when the support set is fixed. To explore many different support sets, we use the blocking method (Method 2) from Section 3.2. Method 2 is much faster than Method 1, so we need to check that it performs similarly, according to both the volume and precision of the approximated Rashomon set. The

volume ratio, defined by $\sqrt[\tilde{K}]{\text{Vol}(\hat{R}_{\text{method1}})/\text{Vol}(\hat{R}_{\text{method2}})}$, should be 1 if the two methods perform similarly. The *precision ratio*, the precision of Method 1 over the precision

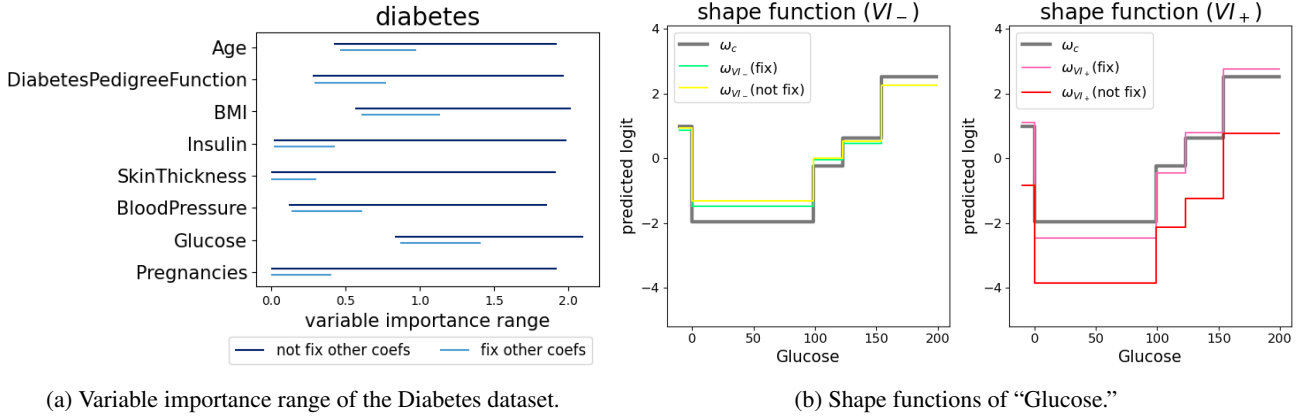


Figure 3. The variable importance range of the Diabetes dataset. “Not fix” means the shape function is obtained by solving Problem (10). “Fix” means coefficients of all other features except “Glucose” are set to the same values as in ω_c . ($\lambda_s = 0.001, \lambda_2 = 0.001, \theta = 1.01\mathcal{L}^*$)

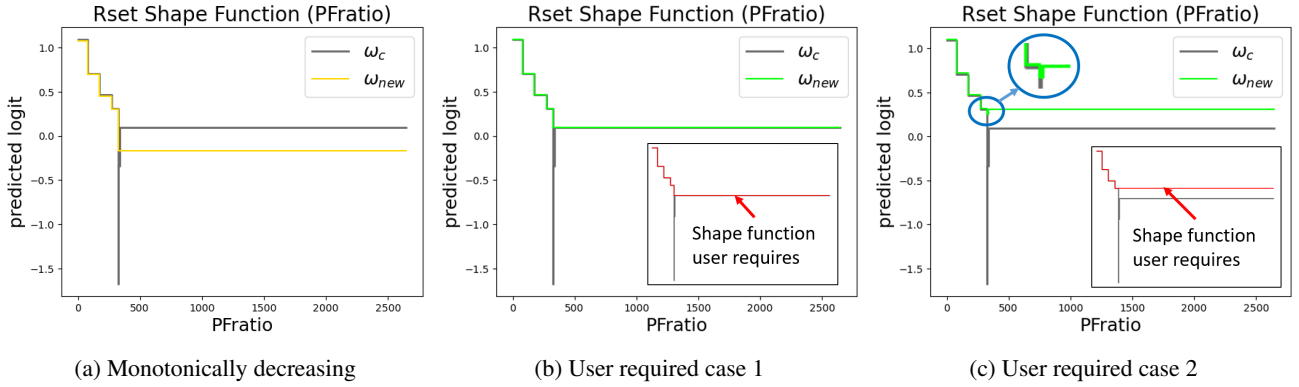


Figure 4. Example shape functions of “PFratio” that satisfy users requirement. (a) The shape function of “PFratio” should be monotonically decreasing. But it has a large jump at PFratio ~ 330 . (b) Algorithm removes the jump by connecting to the right step. (c) Removes the jump by connecting to the left step. ($\lambda_0 = 0.0002, \lambda_2 = 0.001, \theta = 1.01\mathcal{L}^*$).

of Method 2, again should be close to 1 if the methods perform similarly. Figure 2 shows the precision ratio and volume ratio of 100 different new support sets where $u > 0$, i.e., the approximated Rashomon set is non-empty. Clearly, Method 2 will break down if we choose the support size \tilde{K} to be too small. The results from Figure 2 indicate what we expected: precision and volume ratios close to 1, even for relatively small \tilde{K} . Importantly, Method 2 is much more efficient than Method 1. For example, the running time is < 0.001 seconds for Method 2 but ranges from 300 to 1100 seconds for Method 1 on all three datasets (COMPAS, FICO, MIMIC-II). More results are in Appendix C.

5.2. Variable importance range

We solve Problem (9) and (10) to bound the variable importance; results on the Diabetes dataset are shown by dark blue segments in Figure 3a. The light blue segments show the range with an additional constraint that coefficients of features other than the one we are interested in are fixed.

Adding this extra constraint leads to lower VI_+ but has negligible impacts on VI_- . Feature “Glucose” has dominant VI_- and VI_+ compared with other features, indicating that for all well-performing GAMs, this feature is the most important. In fact, the large VI_- indicates that Glucose remains important even in the model that relies least on it in the Rashomon set. This makes sense, because an oral glucose tolerance test indicates diabetes if the plasma glucose concentration is greater than 0 two hours into the test. Features “BMI” and “Age” also have high VI_- , indicating both of them are more important than other features.

Figure 3b shows the shape functions of ω_c and the coefficient vectors obtained when the lowest and highest variable importance are achieved for “Glucose.” All these shape functions follow the same almost-monotonic trend, which means the higher “Glucose” level, the more likely it is that a patient has diabetes. The step occurring when “Glucose” is less than or equal to 0 corresponds to the fact that glucose concentration greater than 0 at 2 hours into an oral

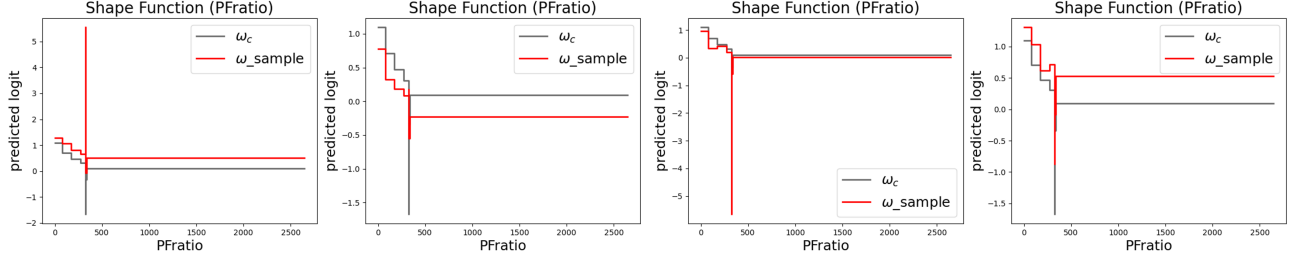


Figure 5. Different shape functions of “PFRatio.”

glucose tolerance test is indicative of diabetes. Shape functions based on ω_{VI+} without fixing other coefficients have a larger magnitude for each step; when we do not fix other coefficients, there is more flexibility in the shape functions.

5.3. User preferred shape functions

A significant advantage of the Rashomon set is that it provides the opportunity for users to contribute their domain knowledge or preferences flexibly without retraining the model. Note that all models within the approximated Rashomon set predict equally well out of sample (see Table 4 in Appendix), so the user can choose any of them. We use feature “PFRatio” in the public MIMIC-II dataset as an example. PFRatio is a measurement of lung function; it measures how well patients convert oxygen from the air into their blood. Missing values commonly exist in the real dataset and imputation is widely used. Chen et al. (2021) uses mean imputation, which often causes sudden jumps in GAMs. Figure 4 shows the shape function of “PFRatio” (in gray), in which a sudden jump occurs when “PFRatio” is around 330. This jump is caused by mean imputation, and has no physical meaning. Since all other steps of this shape function are monotonically decreasing, a potential user requirement might be to make the shape function monotonically decreasing. By solving Problem (11) with the constraint on coefficients related to “PFRatio,” we get the shape function colored in yellow in Figure 4a. The four left steps are only slightly different from ω_c . The jump is reduced while the last step is dragged down by 0.2.

Suppose a user prefers to remove the jump while keeping the last step unchanged (shown in the inset plot in Figure 4b). Fortunately, by solving Problem (12), we find that the specified shape function is within the Rashomon set (shown by the green curve in Figure 4b). Another user might not like this idea, preferring instead to remove the jump by connecting to the left step (shown in the inset plot in Figure 4c). However, this specified shape function is not within the Rashomon set, and we find the closest solution in green, which still has a small jump at 330 (see the inset plot). Different user-specified shape functions lead to different solutions. The approximated Rashomon set can

thus provide a computationally efficient way for users to find models that agree with their expectations, and the data. Tools like GAMChanger (Wang et al., 2021) allows users to directly edit the GAM, but there is no guarantee that models still perform well after editing.

5.4. Changes in shape functions

When we see a jump in the shape function, we might want to know whether this jump commonly exists in other well-performing models. Using the approximated Rashomon set, we can give an answer. For example, we might wonder if the sudden change in the shape function of “PFRatio” in Figure 4a is also present in other well-performing GAMs. We sample 10,000 points from our \hat{R} and find that 7012 samples have a downward jump at the same position. Also, we are surprised to find that in some of the 2988 samples, the jump is instead upward. Figure 5 shows four different shape functions of “PFRatio” sampled from \hat{R} . Note that the diverse set of shape functions is an advantage of the Rashomon set. Using other methods such as logistic regression, which minimizes loss, might always return similar coefficient vectors even with different random seeds.

The dramatic magnitude change in either direction could be caused by the small number of data points falling in this bin ($\pi_{\text{bin}} = 1.2\text{e-}4$). Since the weight is so small, even a tremendous change leads to only a small impact on the loss. In practice, using our proposed optimization methods in Section 4, users can reduce or amplify the jump in the shape function or even create a different curve, as in Figure 4.

6. Conclusion

Our work approximates the Rashomon set of GAMs with a more structured and user-friendly space. This enables users to explore, visualize, modify, and gain insights from the shape functions of GAMs. Our work represents a paradigm shift in machine learning, enabling unprecedented flexibility for users and domain experts to interact with models without compromising performance. Our contributions open a door for enhancing human-model interaction through using the new toolkit provided by the Rashomon set.

References

- Agarwal, R., Melnick, L., Frosst, N., Zhang, X., Lengerich, B., Caruana, R., and Hinton, G. E. Neural additive models: Interpretable machine learning with neural nets. *Advances in Neural Information Processing Systems*, 34: 4699–4711, 2021.
- Agrawal, A., Verschueren, R., Diamond, S., and Boyd, S. A rewriting system for convex optimization problems. *Journal of Control and Decision*, 5(1):42–60, 2018.
- Ahanor, I., Medal, H., and Trapp, A. C. Diversitree: Computing diverse sets of near-optimal solutions to mixed-integer optimization problems. *arXiv preprint arXiv:2204.03822*, 2022.
- Austin, J., Ocker, R., and Bhati, A. Kentucky pretrial risk assessment instrument validation. *Bureau of Justice Statistics*, 2010.
- Borden, H. G. Factors for predicting parole success. *Journal of the American Institute of Criminal Law and Criminology*, pp. 328–336, 1928.
- Breiman, L. Statistical modeling: The two cultures (with comments and a rejoinder by the author). *Statistical science*, 16(3):199–231, 2001.
- Burgess, E. W. Factors determining success or failure on parole. Illinois Committee on Indeterminate-Sentence Law and Parole Springfield, IL, 1928.
- Caruana, R., Lou, Y., Gehrke, J., Koch, P., Sturm, M., and Elhadad, N. Intelligible models for healthcare: Predicting pneumonia risk and hospital 30-day readmission. In *Proceedings of the 21th ACM SIGKDD international conference on knowledge discovery and data mining*, pp. 1721–1730, 2015.
- Chen, Z., Tan, S., Nori, H., Inkpen, K., Lou, Y., and Caruana, R. Using explainable boosting machines (ebms) to detect common flaws in data. In *Joint European Conference on Machine Learning and Knowledge Discovery in Databases*, pp. 534–551. Springer, 2021.
- Coker, B., Rudin, C., and King, G. A theory of statistical inference for ensuring the robustness of scientific results. *Management Science*, 67(10):6174–6197, 2021.
- Danna, E., Fenelon, M., Gu, Z., and Wunderling, R. Generating multiple solutions for mixed integer programming problems. In *International Conference on Integer Programming and Combinatorial Optimization*, pp. 280–294. Springer, 2007.
- Diamond, S. and Boyd, S. CVXPY: A Python-embedded modeling language for convex optimization. *Journal of Machine Learning Research*, 17(83):1–5, 2016.
- Dong, J. and Rudin, C. Exploring the cloud of variable importance for the set of all good models. *Nature Machine Intelligence*, 2(12):810–824, 2020.
- D’Amour, A., Heller, K., Moldovan, D., Adlam, B., Alipanahi, B., Beutel, A., Chen, C., Deaton, J., Eisenstein, J., Hoffman, M. D., et al. Underspecification presents challenges for credibility in modern machine learning. *Journal of Machine Learning Research*, 2020.
- FICO, Google, Imperial College London, MIT, University of Oxford, UC Irvine, and UC Berkeley. Explainable Machine Learning Challenge. <https://community.fico.com/s/explainable-machine-learning-challenge>, 2018.
- Fisher, A., Rudin, C., and Dominici, F. All models are wrong, but many are useful: Learning a variable’s importance by studying an entire class of prediction models simultaneously. *J. Mach. Learn. Res.*, 20(177):1–81, 2019.
- Hara, S. and Ishihata, M. Approximate and exact enumeration of rule models. In *Proceedings of the AAAI Conference on Artificial Intelligence*, volume 32, 2018.
- Hara, S. and Maehara, T. Enumerate lasso solutions for feature selection. In *Proceedings of the AAAI Conference on Artificial Intelligence*, volume 31, 2017.
- Hastie, T. and Tibshirani, R. *Generalized Additive Models*, volume 43. CRC Press, 1990.
- Hsu, H. and Calmon, F. d. P. Rashomon capacity: A metric for predictive multiplicity in probabilistic classification. *arXiv preprint arXiv:2206.01295*, 2022.
- Kessler, R. C., Adler, L., Ames, M., Demler, O., Faraone, S., Hiripi, E., Howes, M. J., Jin, R., Secnik, K., Spencer, T., et al. The world health organization adult adhd self-report scale (asrs): a short screening scale for use in the general population. *Psychological medicine*, 35(2): 245–256, 2005.
- Kissel, N. and Mentch, L. Forward stability and model path selection. *arXiv preprint arXiv:2103.03462*, 2021.
- Larson, J., Mattu, S., Kirchner, L., and Angwin, J. How we analyzed the COMPAS recidivism algorithm. *ProPublica*, 2016.
- Latessa, E. J., Lemke, R., Makarios, M., and Smith, P. The creation and validation of the ohio risk assessment system (oras). *Fed. Probation*, 74:16, 2010.
- Lengerich, B. J., Nunnally, M. E., Aphinyanaphongs, Y., Ellington, C., and Caruana, R. Automated interpretable

- discovery of heterogeneous treatment effectiveness: A covid-19 case study. *Journal of biomedical informatics*, 130:104086, 2022.
- Liu, J., Zhong, C., Seltzer, M., and Rudin, C. Fast sparse classification for generalized linear and additive models. *Proceedings of machine learning research*, 151:9304, 2022.
- Lou, Y., Caruana, R., Gehrke, J., and Hooker, G. Accurate intelligible models with pairwise interactions. In *Proceedings of the 19th ACM SIGKDD international conference on Knowledge discovery and data mining*, pp. 623–631, 2013.
- Marx, C., Calmon, F., and Ustun, B. Predictive multiplicity in classification. In *International Conference on Machine Learning*, pp. 6765–6774. PMLR, 2020.
- Moreno, R. P., Metnitz, P. G., Almeida, E., Jordan, B., Bauer, P., Campos, R. A., Iapichino, G., Edbrooke, D., Capuzzo, M., Le Gall, J.-R., et al. Saps 3—from evaluation of the patient to evaluation of the intensive care unit. part 2: Development of a prognostic model for hospital mortality at icu admission. *Intensive care medicine*, 31:1345–1355, 2005.
- Nori, H., Jenkins, S., Koch, P., and Caruana, R. Interpretml: A unified framework for machine learning interpretability. *arXiv preprint arXiv:1909.09223*, 2019.
- Ruggieri, S. Enumerating distinct decision trees. In *International Conference on Machine Learning*, pp. 2960–2968. PMLR, 2017.
- Ruggieri, S. Complete search for feature selection in decision trees. *J. Mach. Learn. Res.*, 20:104–1, 2019.
- Saeed, M., Lieu, C., Raber, G., and Mark, R. G. Mimic ii: a massive temporal icu patient database to support research in intelligent patient monitoring. In *Computers in cardiology*, pp. 641–644. IEEE, 2002.
- Semenova, L., Rudin, C., and Parr, R. On the existence of simpler machine learning models. In *ACM Conference on Fairness, Accountability, and Transparency (ACM FAccT)*, 2022.
- Six, A., Backus, B., and Kelder, J. Chest pain in the emergency room: value of the heart score. *Netherlands Heart Journal*, 16(6):191–196, 2008.
- Smith, G., Mansilla, R., and Goulding, J. Model class reliance for random forests. *Advances in Neural Information Processing Systems*, 33:22305–22315, 2020.
- Smith, J. W., Everhart, J. E., Dickson, W., Knowler, W. C., and Johannes, R. S. Using the adap learning algorithm to forecast the onset of diabetes mellitus. In *Proceedings of the annual symposium on computer application in medical care*, pp. 261. American Medical Informatics Association, 1988.
- Todd, M. J. and Yıldırım, E. A. On khachiyan’s algorithm for the computation of minimum-volume enclosing ellipsoids. *Discrete Applied Mathematics*, 155(13):1731–1744, 2007.
- Tulabandhula, T. and Rudin, C. Robust optimization using machine learning for uncertainty sets. *arXiv preprint arXiv:1407.1097*, 2014.
- Wang, Z. J., Kale, A., Nori, H., Stella, P., Nunnally, M., Chau, D. H., Vorvoreanu, M., Vaughan, J. W., and Caruana, R. Gam changer: Editing generalized additive models with interactive visualization. *arXiv preprint arXiv:2112.03245*, 2021.
- Xin, R., Zhong, C., Chen, Z., Takagi, T., Seltzer, M., and Rudin, C. Exploring the whole rashomon set of sparse decision trees. *arXiv preprint arXiv:2209.08040*, 2022.

A. Summary of datasets

We show experimental results on four datasets: a recidivism dataset (COMPAS) (Larson et al., 2016), the Fair Isaac (FICO) credit risk dataset (FICO et al., 2018) used for the Explainable ML Challenge, the Diabetes dataset (Smith et al., 1988), and an ICU dataset MIMIC-II (Saeed et al., 2002). Table 1 summarizes all the datasets.

Dataset	Samples	Features	Classification task
COMPAS	6907	7	Predict if someone will be arrested ≤ 2 years of release
FICO	10459	23	Predict if someone will default on a loan
Diabetes	768	9	Predict whether a pregnant woman has diabetes
MIMIC-II	24508	17	Predict whether a patient dies in ICU

Table 1. Summary of datasets

B. Sampling Uniformly from Ellipsoid

Algorithm 1 *SampleFromEllipsoid*(\mathbf{Q}, ω_c)

Input: parameters of the ellipsoid $\mathbf{Q} \in \mathbb{R}^{m \times m}$, $\omega_c \in \mathbb{R}^m$

Output: a point inside the ellipsoid $\omega \in \mathbb{R}^m$

```

1:  $\mathbf{u} \sim \mathcal{N}(\mathbf{0}, \mathbf{I})$  // sample a  $m$  dimensional vector from standard multivariate Gaussian distribution
2:  $\mathbf{u} \leftarrow \mathbf{u} / \|\mathbf{u}\|_2$  // normalize it to get a unit-vector
3:  $r \sim U(0, 1)$  // get a sample from uniform distribution
4:  $r \leftarrow r^{1/m}$  // rescale to get the radius of a sample in a unit sphere
5:  $\mathbf{y} \leftarrow r\mathbf{u}$  //  $\mathbf{y}$  is a random point inside a unit sphere
6:  $\mathbf{\Lambda}, \mathbf{V} = \text{Eig}(\mathbf{Q})$  // Eigen-decomposition, diagonal of  $\mathbf{\Lambda}$  are the eigenvalues, and columns of  $\mathbf{V}$  are eigenvectors
7:  $\mathbf{x} \leftarrow \mathbf{\Lambda}^{-\frac{1}{2}} \mathbf{V}^T \mathbf{y}$  // get a point in the ellipsoid  $\mathbf{x}^T \mathbf{Q} \mathbf{x} \leq 1$ 
8:  $\omega = \mathbf{x} + \omega_c$  // shift it so that the center is  $\omega_c$ 
return  $\omega$ 
    
```

Algorithm 1 describes the algorithm to uniformly sample from the ellipsoid $\{\omega \in \mathbb{R}^m : (\omega - \omega_c)^T \mathbf{Q} (\omega - \omega_c) \leq 1\}$. The algorithm first samples a random point inside a high dimensional unit sphere (line 1-5), and applies linear transformation (calculated from \mathbf{Q} and ω_c) to get the point in the target ellipsoid (line 6-8). The whole process can be decomposed into a purely stochastic part, i.e., sample in the unit sphere, and a deterministic part which is differentiable. Using this sampling algorithm, we can get samples for objective 6 and use gradient-based methods to optimize \mathbf{Q} and ω_c . In addition, the algorithm is also used to sample data for the problem in Section 4.3, and to calculate precisions in Section 5.1.

C. Precision and volume of the approximated Rashomon set

To run our method, we set the learning rate to 0.0001 and run 1000 iterations. C is set to 500. For the logistic regression and EBM baselines, we sample 2000 coefficient vectors by fitting GAMs on the bootstrap sampled subsets of data. We run logistic regression with ℓ_2 penalty and EBM with no interaction terms. We then find the minimum volume ellipsoid that can cover most coefficient vectors. Given a set of coefficient vectors ω_{samples} , we solve the following problem:

$$\min_{\mathbf{Q}, \omega_c} -\det(\mathbf{Q})^{\frac{1}{2m}} + C \cdot \frac{1}{2000} \sum_{i=1}^{2000} \max(\|\mathbf{Q}^{1/2}(\omega_{\text{sample}_i} - \omega_c)\|^2 - 1, 0). \quad (13)$$

We solve this problem via gradient descent. C is set to 1000. The number of iterations and learning rate in GD are set to 1000 and 0.01, respectively. We initialize \mathbf{Q} by the ZCA whitening matrix and ω_c by the average of ω_{samples} .

After rescaling the Rashomon set approximated by baselines, we sample 10,000 points from our \hat{R} and rescaled baseline Rashomon sets, calculate the loss, and get the precision. We include more figures in this appendix that are similar to Figure 1 to compare with baselines using different values of λ_s and θ .

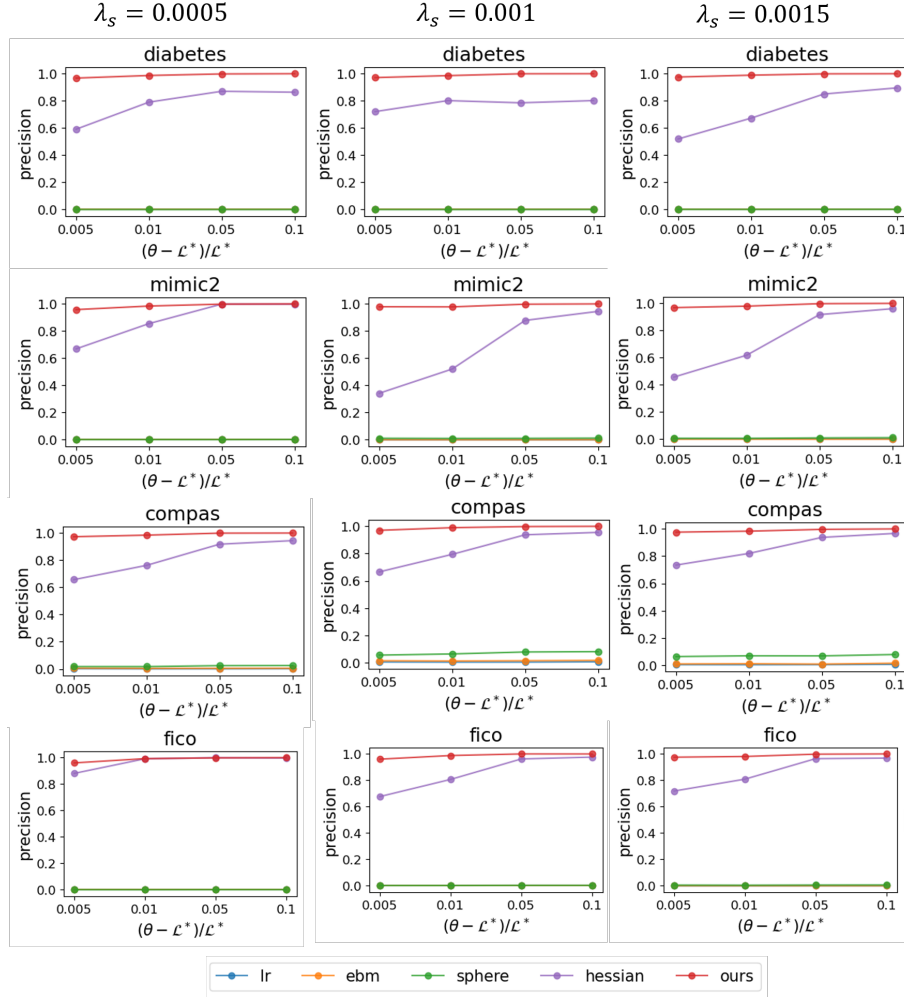


Figure 6. Precision of the approximated Rashomon sets as a function of θ . Our method always dominates other baselines.

Figure 6 compares the precision of our method and baselines when the volume is fixed. The Rashomon set approximated by our method has the largest intersection with the true Rashomon set. And this pattern is consistent across all datasets and values of λ_s . The Rashomon set approximated by hessian has lower precision but is always better than the other baselines. As θ becomes larger, the hessian method becomes better and sometimes comes close to the result after optimization.

Figure 7 shows the tradeoff between the size and precision of the approximated Rashomon set for each method. The Rashomon set approximated by our optimization method is better than baselines given different values of θ .

GAMs with different Support Sets: In these experiments, we keep 90%, 80%, and 70% of bins trained with $\lambda_s = 0.0005$, $\lambda_2 = 0.001$. For the baseline method, C is set to 3000, and the learning rate and the number of iterations are set to 0.001 and 2500, respectively. Since $\binom{K-p}{K-K}$ could be very large, we first sample 10,000 different merging strategies and compare at most 100 R_{P_S} . Table 2 shows more detailed results. Merging 30% of bins for the MIMIC-II dataset leads to empty R_{P_S} for 10,000 merging strategies and merging bins for the Diabetes dataset also leads to empty R_{P_S} .

D. Variable importance range

In this section, we first show more results on variable importance range and then compare the timing for obtaining VI_+ .

We show the shape functions of “Glucose” when the lowest and highest variable importance are achieved in Figure 3. When the importance of “Glucose” is minimized or maximized, one might be interested in how the shape function changes for

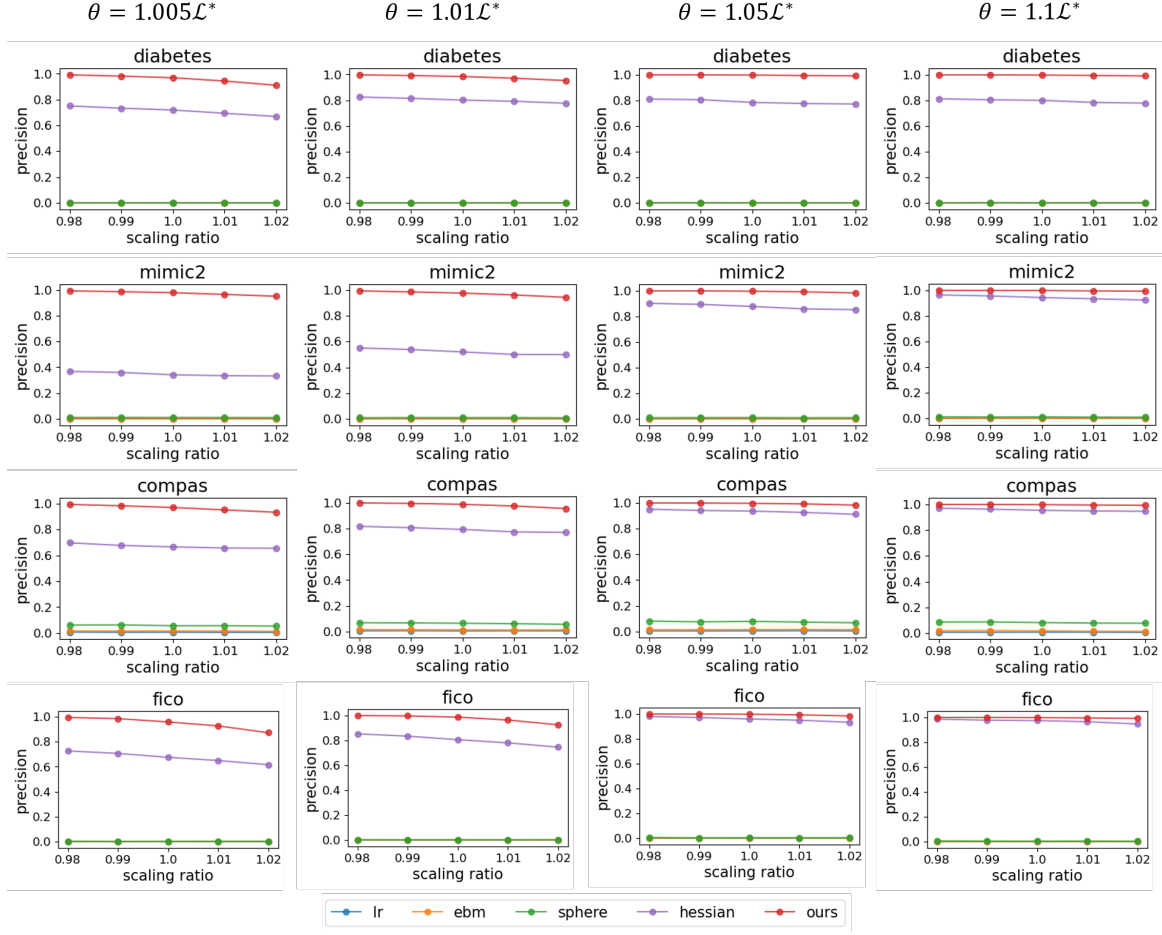


Figure 7. Tradeoff between precision and the size of the approximated Rashomon set given different θ .

other features. We show such variations in Figure 8. Most features keep the trend as ω_c with some variation in magnitude.

Figure 9 shows the variable importance range on the MIMIC-II, FICO, and COMPAS datasets. For the MIMIC-II dataset (left subfigure), features “PFRatio”, “GCS”, and “Age” have relatively higher VI_- , which means these features are in general important for GAMs in the Rashomon set. For the FICO dataset (mid subfigure), features “ExternalRiskEstimate” and “MSinceMostRecentInqexcl7days” have higher VI_- either fixing or not fixing other coefficients, indicating that these two features are important. Feature “prior_count” in the COMPAS dataset has slightly higher VI_- than feature “age.”

As we mentioned in Section 4.1, the lower bound of variable importance VI_- is obtained by solving a linear programming problem with a quadratic constraint, while to get the upper bound of variable importance we need to solve a mixed integer programming problem. We use Python CVXPY package (Diamond & Boyd, 2016; Agrawal et al., 2018) for solving LP problems and Cplex 12.8 for MIP problems. Since solving a MIP problem is usually time-consuming, we also propose another way to get VI_+ . Note that it’s the absolute value in the objective that restricts us to use LP solver. Therefore, we enumerate all positive-negative combinations of $\omega_{j,k}$, $k \in \{0, B_j - 1\}$, and then solve LP problem with the sign constraint enforced (see Algorithm 2). Table 3 compares the running time by solving MIP and LP problem for VI_+ . Time consumption for solving LP problem with the sign constraint enforced is usually less than solving a MIP problem.

E. Shape functions of GAMs in the Rashomon set

Next, we show a diverse set of coefficient vectors sampled from the approximated Rashomon set. Figure 10 and Figure 11 depict 100 coefficient vectors (in red) sampled from the ellipsoid and ω_c (in gray), the center of the optimized ellipsoid of the Diabetes and MIMIC-II dataset, respectively. Various different red lines in each subfigure indicate that the approximated

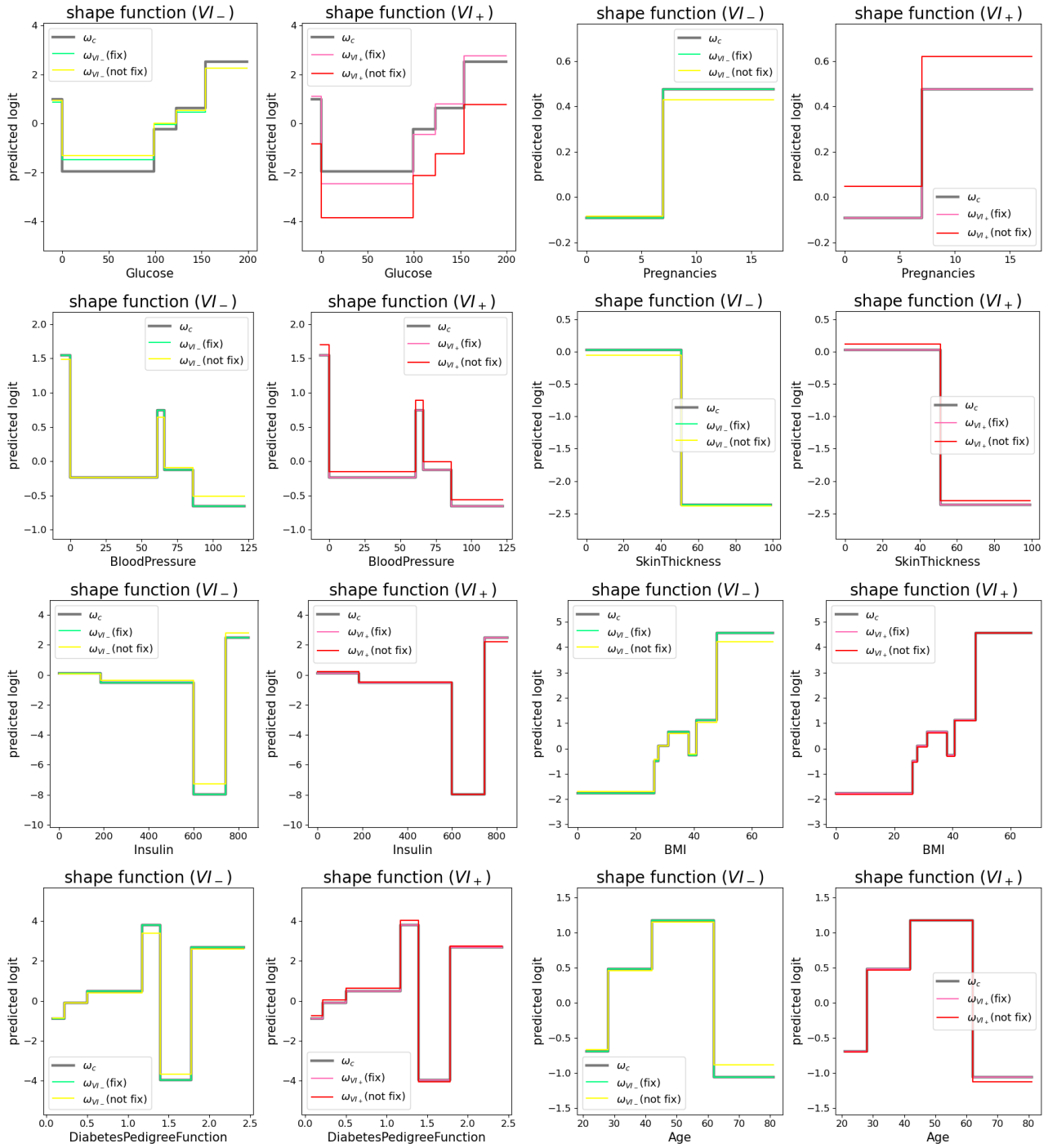


Figure 8. Shape functions of other features in the Diabetes dataset when the importance of “Glucose” is minimized or maximized.

Dataset	\tilde{K}	precision ratio	volume ratio	time ours (sec)	time baseline (sec)
COMPAS	15	1.01 ± 0.03	1.05 ± 0.07	$4.84\text{e-}4 \pm 6.25\text{e-}5$	324.85 ± 8.70
COMPAS	14	1.01 ± 0.05	1.12 ± 0.12	$4.76\text{e-}4 \pm 9.33\text{e-}5$	296.51 ± 41.46
COMPAS	13	0.99 ± 0.01	1.20 ± 0.12	$4.77\text{e-}4 \pm 1.13\text{e-}4$	272.64 ± 6.64
FICO	28	1.01 ± 0.04	0.90 ± 0.06	$9.99\text{e-}4 \pm 4.54\text{e-}3$	377.10 ± 14.95
FICO	26	0.99 ± 0.06	1.10 ± 0.13	$5.59\text{e-}4 \pm 1.12\text{e-}4$	374.28 ± 10.24
FICO	24	0.99 ± 0.02	1.29 ± 0.13	$5.55\text{e-}4 \pm 4.04\text{e-}5$	297.15 ± 8.26
MIMIC-II	35	1.00 ± 0.20	0.93 ± 0.10	$5.89\text{e-}4 \pm 1.72\text{e-}4$	1127.10 ± 141.42
MIMIC-II	32	0.99 ± 0.01	1.10 ± 0.06	$5.29\text{e-}4 \pm 2.76\text{e-}5$	1067.50 ± 12.90

Table 2. Precision, volume, and time comparison between blocking method (Method 2) and optimization (Method 1).

Algorithm 2 $GetVI_{+}FromLP(\pi_j, \mathbf{Q}, \omega_c)$

Input: proportion of samples in each bin of feature j $\pi_j \in \mathbb{R}^{B_j}$, parameters of the ellipsoid $\mathbf{Q} \in \mathbb{R}^{m \times m}$, $\omega_c \in \mathbb{R}^m$

Output: a point inside the ellipsoid $\omega \in \mathbb{R}^m$

```

1:  $Obj^* \leftarrow -\infty$ 
2: for  $I \in \{-1, 1\}^{B_j}$  // try all positive-negative combinations for  $\omega_{j,k}, k \in \{0, \dots, B_j - 1\}$ 
    // solve the LP problem
3:    $Obj, \omega \leftarrow \max_{\omega_j} (\pi_j \odot I)^T \omega_j$  such that  $(\omega - \omega_c)^T \mathbf{Q} (\omega - \omega_c) \leq 1$ 
4:   if  $Obj > Obj^*$ :
5:      $\omega^* \leftarrow \omega, Obj^* \leftarrow Obj$ 
6: return  $\omega^*$ 
    
```

Rashomon set contains many different coefficient vectors. And these models are actually within the true Rashomon sets. Many of them may generally follow similar patterns as we can see from the trend of these shape functions, while some of them may have some variations (see Figure 5). In summary, using the approximated Rashomon set, we can easily get a diverse set of shape functions for each feature.

F. User preferred shape functions

In real applications, users might have preference for shape functions that are consistent with their domain knowledge. Our approximated Rashomon set makes it easy to incorporate such user preferences by finding a model within the set that satisfies some constraints. We show two case studies here.

Diabetes: There is a jump in the shape function of “BMI” in Figure 10. One possible user requirement might be making this BMI shape function monotonically increasing. By solving the quadratic programming problem with linear constraints, we can get the shape functions shown in Figure 12a. The updated shape function for “BMI” is monotonically increasing (in

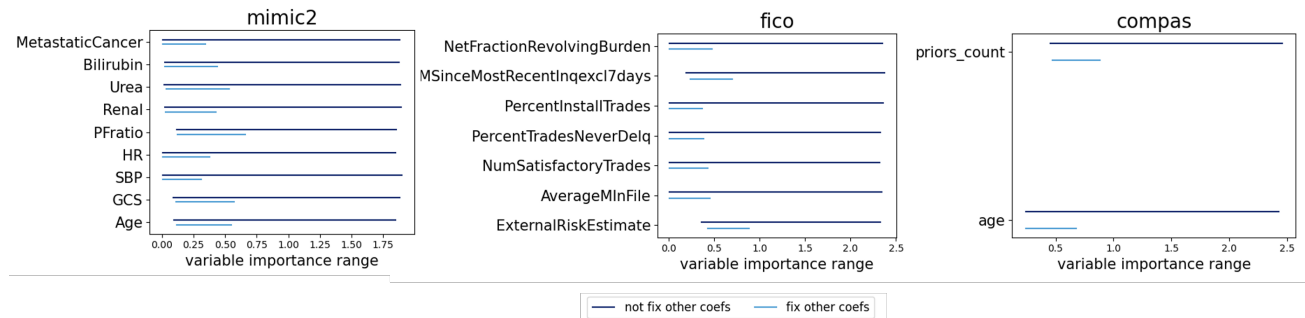


Figure 9. The variable importance range of the MIMIC-II, FICO, and COMPAS datasets. Each line connects VI_- and VI_+ . ($\lambda_s = 0.001, \lambda_2 = 0.001, \theta = 1.01\mathcal{L}^*$)

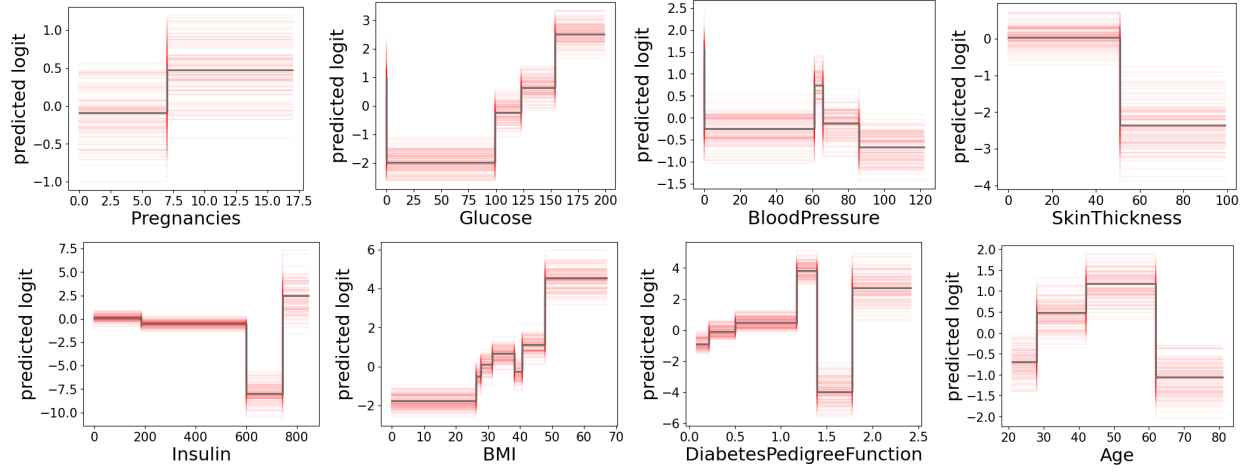


Figure 10. 100 different shape functions of the Diabetes dataset. The shape function at ω_c is colored in gray. ($\lambda_s = 0.001, \lambda_2 = 0.001, \theta = 1.01\mathcal{L}^*$)

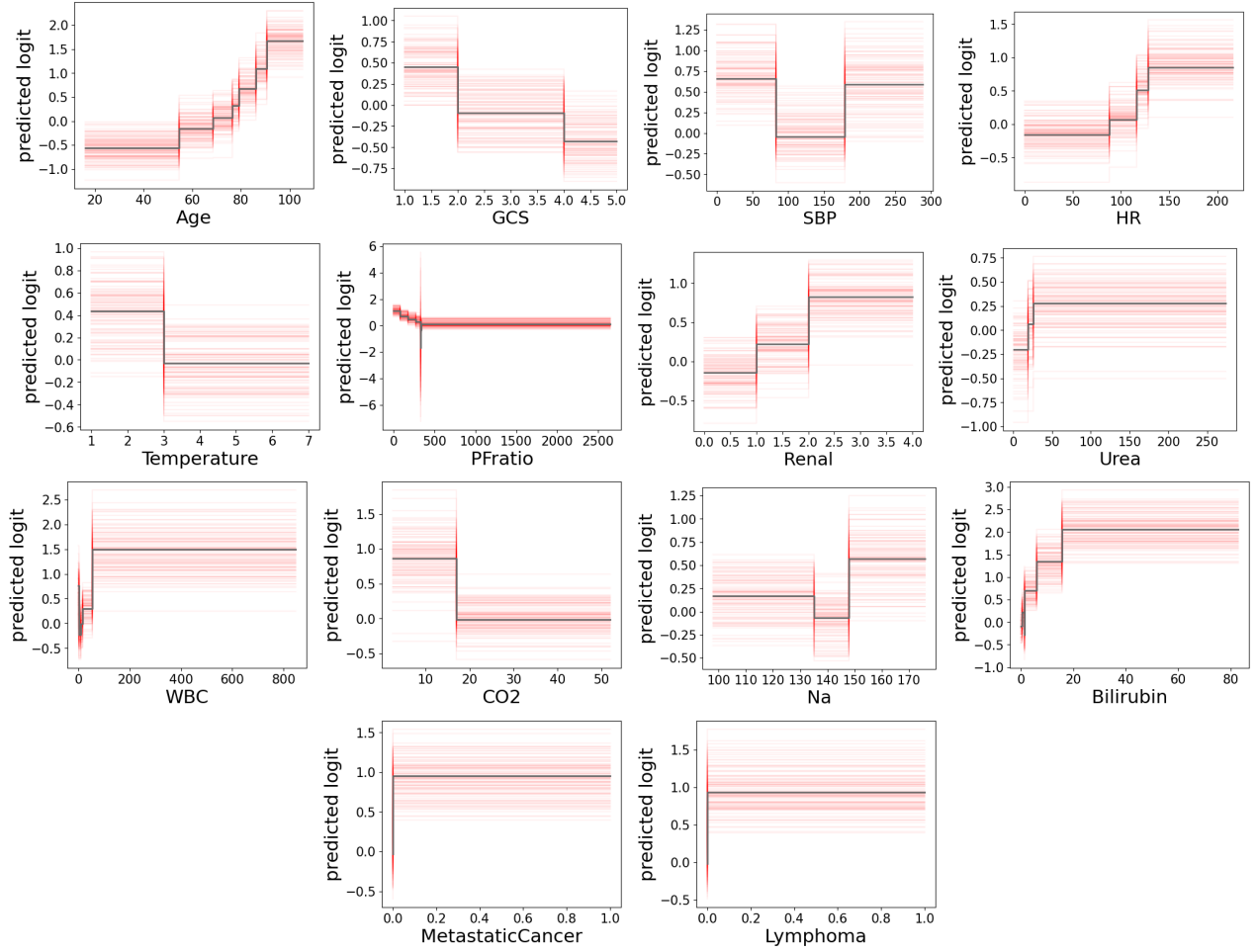


Figure 11. 100 different shape functions of the MIMIC-II dataset. The shape function at ω_c is colored in gray. ($\lambda_s = 0.0002, \lambda_2 = 0.001, \theta = 1.01\mathcal{L}^*$)

Dataset	Fix other coefs		Not fix other coefs	
	MIP	LP	MIP	LP
Diabetes	18.876 ± 10.025	4.780 ± 4.996	35.597 ± 17.413	1.961 ± 2.164
MIMIC-II	11.450 ± 6.259	0.497 ± 0.166	14.977 ± 12.921	0.265 ± 0.139
COMPAS	23.193 ± 0.176	4.138 ± 0.033	46.782 ± 5.709	3.043 ± 0.017
FICO	11.749 ± 7.841	0.816 ± 0.766	30.133 ± 7.11	0.425 ± 0.457

Table 3. Time comparison in seconds between solving MIP and LP problem with the sign constraint enforced for VI_+ .

yellow). With the constraint, the sudden decrease that occurs at “BMI”=40 is removed by connecting the left step. Because of the change imposed on “BMI”, the shape functions of other features are also updated. Almost all of them follow the trend in ω_c with small changes in magnitude. Note that this optimization problem is solved in 0.0007 seconds.

One might also be interested in making the shape function of “DiabetesPedigreeFunction” monotonically increasing. Smith et al. (1988) developed the Diabetes Pedigree Function (DPF) to provide a synthesis of the diabetes mellitus history in relatives and the genetic relationship of those relatives to the subject. In general, the DPF increases as the number of relatives who developed diabetes increases, as the age at which those relatives developed diabetes decreases, and as the percentage of genes that they share with the subject increases.

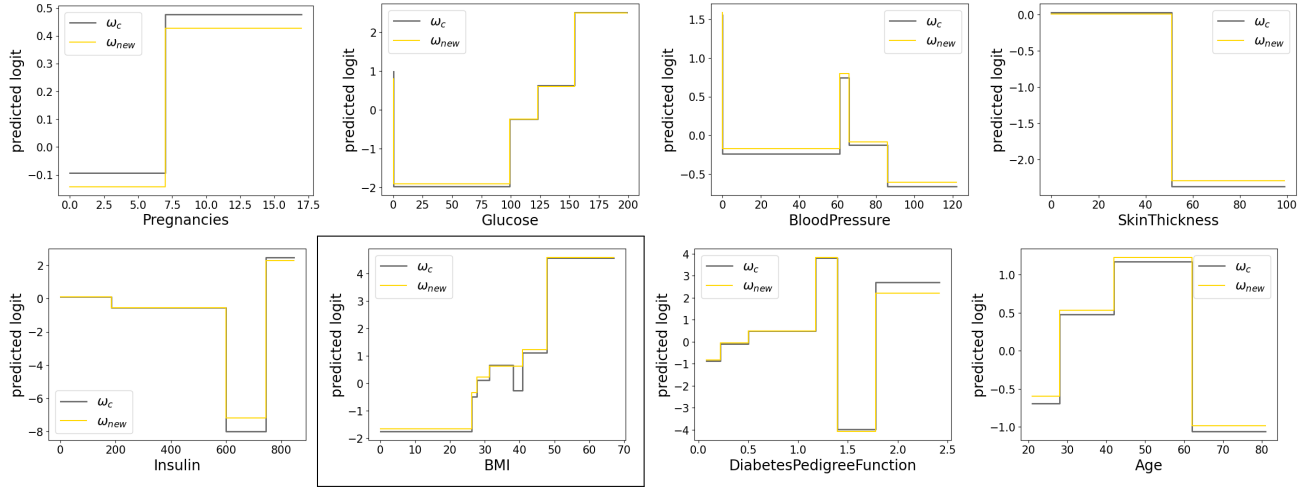
The yellow curves in Figure 12b show the updated shape functions after solving the optimization problem. The shape function of “DiabetesPedigreeFunction” is now monotonically increasing. Similar to Figure 12a, the updated shape functions of other features follow the trend in ω_c with small changes in magnitude. And this optimization problem is solved in 0.0006 seconds.

Sometimes a monotonic constraint is not what users want; they might have more specific preferences on the shape functions. Here we show some examples using hypothetical shape functions. Figure 13 shows shape functions after imposing two different requirements on “BMI.” In Figure 13a, the required shape function of “BMI” (colored in red in the top-left subfigure) shifts below ω_c but is monotonically increasing. Though the closest shape function in the approximated Rashomon set is also below ω_c , it’s not necessarily monotonically increasing. It’s more likely to match the trend in ω_c , because we try to minimize the Euclidean distance between the required shape function and the shape function in \hat{R} . Shape functions of other features change only slightly in magnitude.

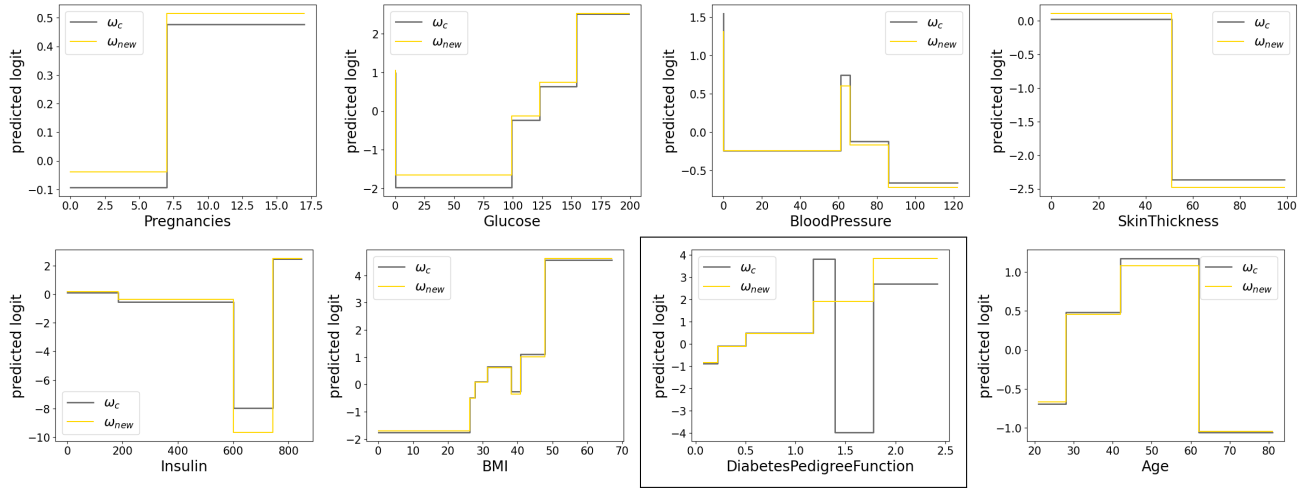
Figure 13b shows an extreme case. The required shape function of “BMI” is totally different from ω_c . But after solving the QP problem, the updated shape function shown in green in the top-middle subfigure has a similar trend to ω_c .

MIMIC-II: In Figure 11, we can see jumps in several shape functions. We can impose monotonic constraints on two features “PFRatio” and “Bilirubin” simultaneously. We want the shape function of “PFRatio” to be monotonically decreasing, while the shape function of “Bilirubin” is monotonically increasing. Figure 14 shows the shape functions after optimization. The shape functions of “PFRatio” and “Bilirubin” satisfy the requirement as shown in the inset plots, and the shape functions of other features are only slightly changed.

Suppose a user prefers to remove the jump in the shape function of “PFRatio.” One way is to remove the jump while keeping the last step unchanged (top-left subfigure in Figure 15a). Fortunately, by solving Problem (12), we find that the specified shape function is within the Rashomon set (shown by the green curve in the top-mid subfigure in Figure 15a). Another user might not like this idea and prefers to remove the jump by connecting to the left step (Figure 15b). However, this specified shape function is not within the Rashomon set, and we find the closest solution in green, which still has a small jump at 330 (see the inset plot). Different user-specified shape functions lead to different solutions. The Rashomon set can serve as a small but computationally efficient space in which users can find a model that is closest to their needs.

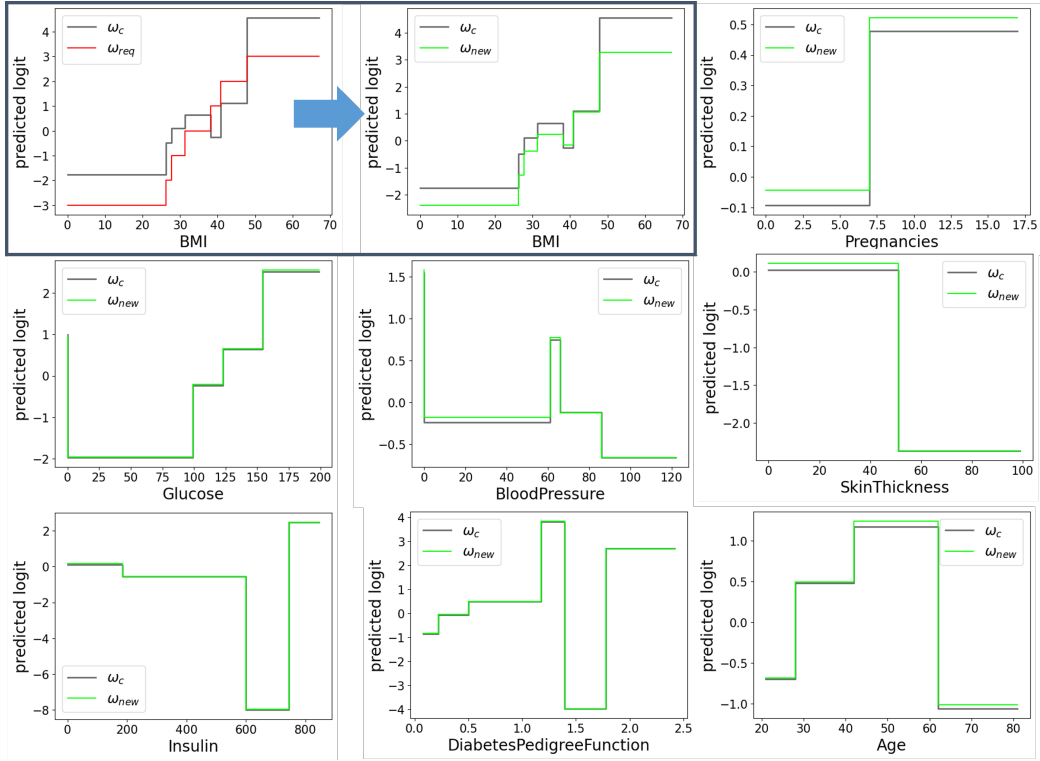


(a) Shape functions of the Diabetes dataset with the monotonic constraint on the “BMI” (in yellow). The optimization problem is solved in 0.0007 seconds.

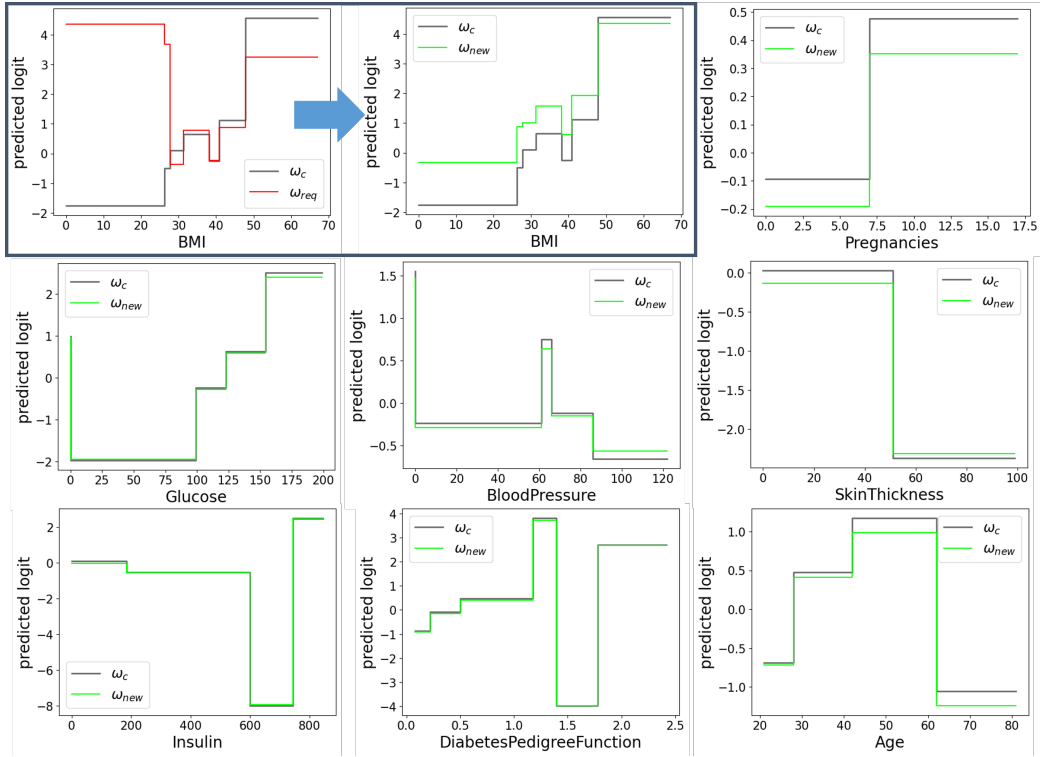


(b) Shape functions of the Diabetes dataset with the monotonic constraint on the “DiabetesPedigreeFunction” (in yellow). The optimization problem is solved in 0.0006 seconds.

Figure 12. Shape functions with monotonic constraints.



(a) Case 1



(b) Case 2

Figure 13. Shape functions on the Diabetes dataset after a hypothetical shape function on “BMI” is required. The red curve in the top-left subfigure is the required shape function. The shape function colored in green in the top-middle subfigure is the closest shape function within \hat{R} .

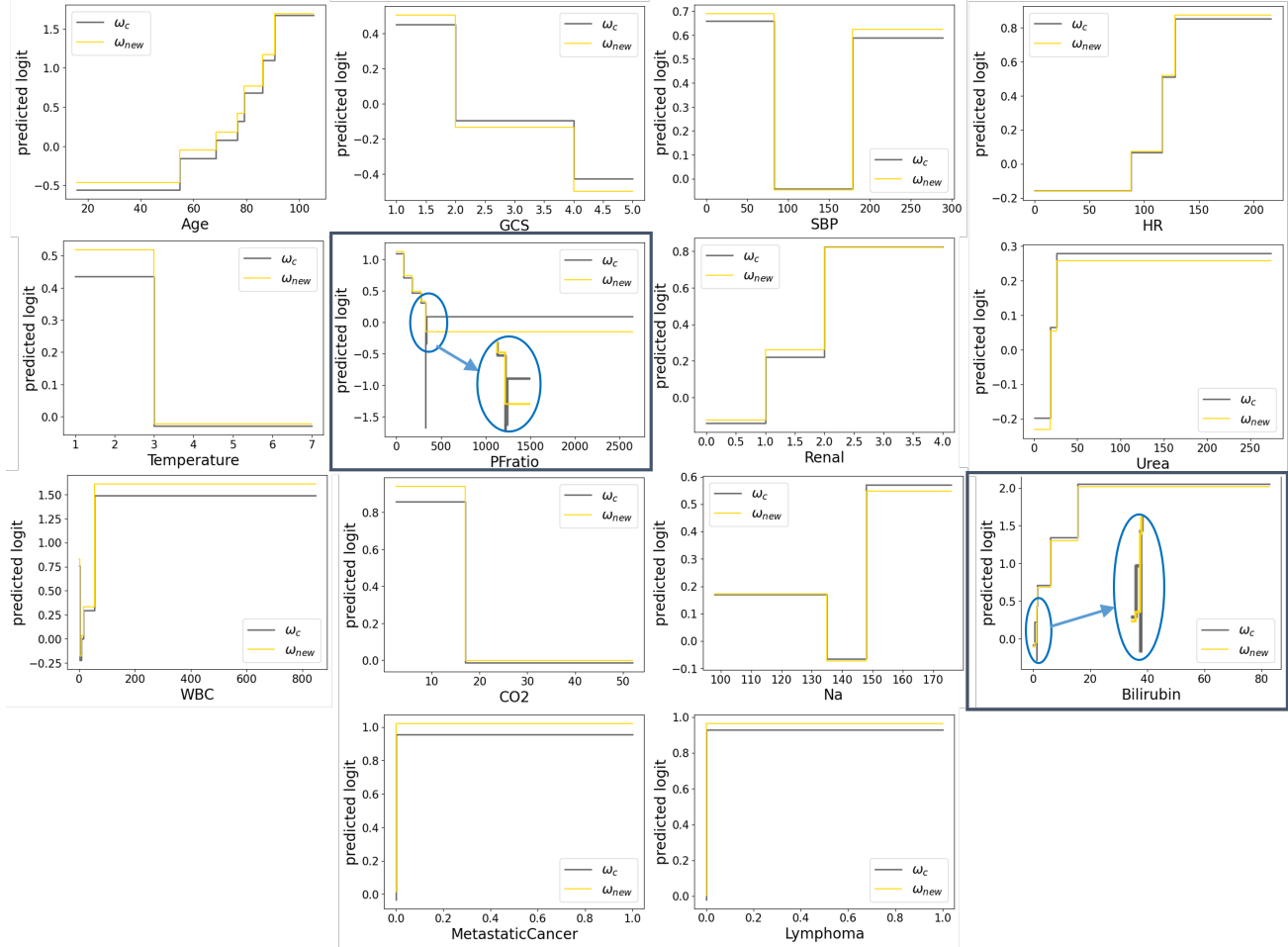


Figure 14. Shape functions of the MIMIC-II dataset with the monotonic constraints on the “PFRatio” and “Bilirubin” (in yellow).

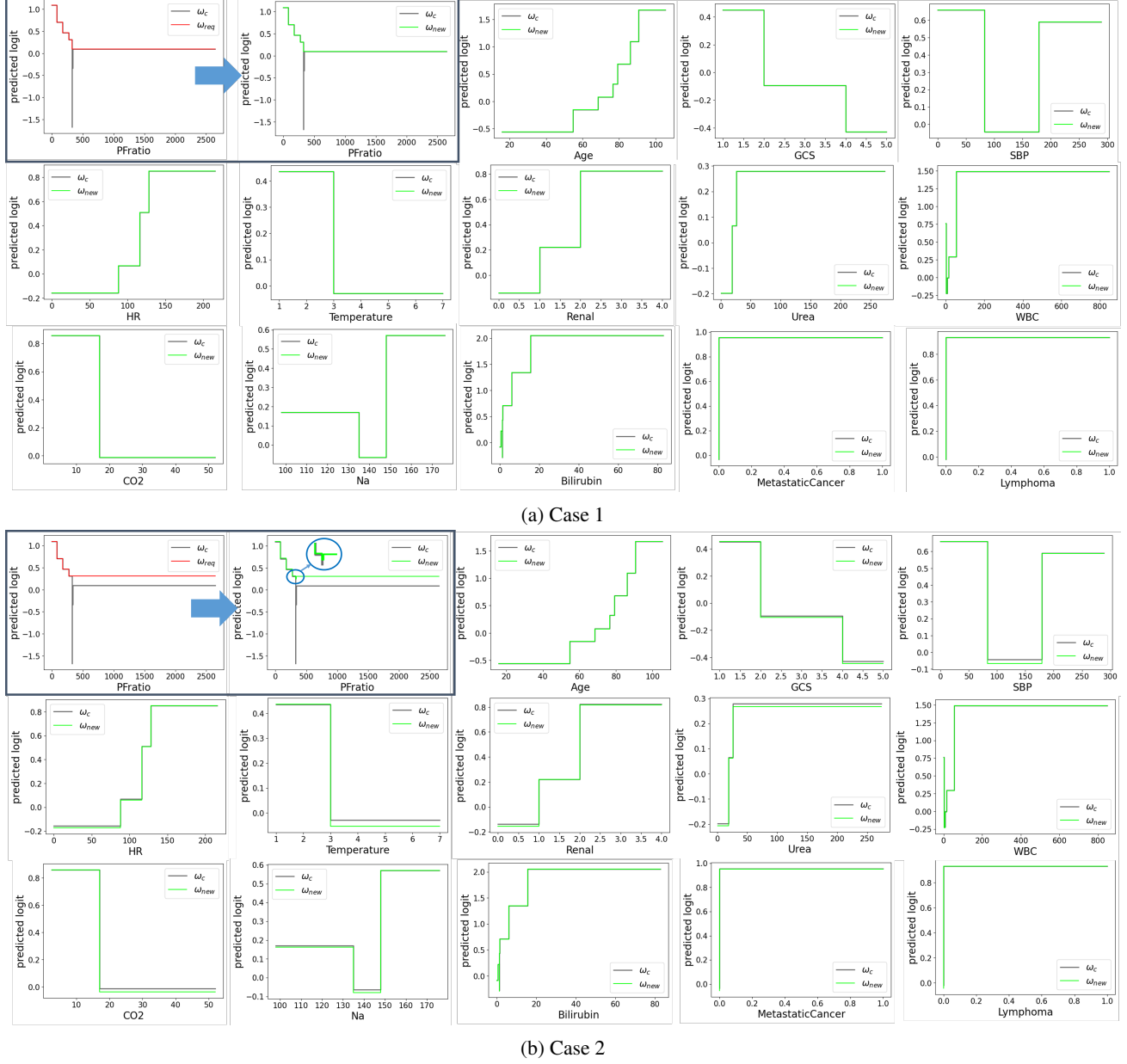


Figure 15. Shape functions on the MIMIC-II dataset after a hypothetical shape function on “PFRatio” is required. The red curve in the top-left subfigure is the required shape function. The shape function colored in green in the top-middle subfigure is the closest shape function within $\hat{\mathcal{R}}$.

Dataset	θ (constant * \mathcal{L}^*)	ω^*		ω sampled from \hat{R}	
		accuracy	auc	accuracy	auc
COMPAS	1.005	0.696	0.748	0.683 ± 0.010	0.744 ± 0.004
	1.01			0.683 ± 0.010	0.742 ± 0.005
	1.05			0.668 ± 0.017	0.724 ± 0.012
	1.1			0.649 ± 0.026	0.704 ± 0.021
FICO	1.005	0.720	0.792	0.717 ± 0.003	0.791 ± 0.001
	1.01			0.716 ± 0.004	0.790 ± 0.002
	1.05			0.708 ± 0.008	0.780 ± 0.006
	1.1			0.700 ± 0.010	0.770 ± 0.009
Diabetes	1.005	0.760	0.819	0.761 ± 0.004	0.818 ± 0.002
	1.01			0.760 ± 0.005	0.818 ± 0.003
	1.05			0.758 ± 0.011	0.816 ± 0.006
	1.1			0.755 ± 0.014	0.814 ± 0.009
MIMIC-II	1.005	0.886	0.803	0.886 ± 0.001	0.803 ± 0.002
	1.01			0.886 ± 0.001	0.802 ± 0.002
	1.05			0.885 ± 0.002	0.794 ± 0.005
	1.1			0.884 ± 0.003	0.784 ± 0.009

Table 4. Test accuracy and AUC comparison between ω^* and ω sampled from the approximated Rashomon set with respect to different θ s.

G. Test performance

We now show the test performance of models sampled from our approximated Rashomon set. We compare the test accuracy and AUC between ω^* and ω s sampled from \hat{R} on the four datasets with different values of θ and results are shown in Table 4. We sample 1000 ω from \hat{R} and show the average and one standard deviation. The larger value of θ leads to a larger Rashomon set, which means we allow models with higher loss. Therefore, as θ increases, both accuracy and AUC decrease. But when the constant is slightly larger than 1, such as 1.005 and 1.01, the test performance of models sampled from \hat{R} usually covers the performance achieved by ω^* in one standard deviation. This means in general our approximated Rashomon set can return a diverse set of models without compromising the performance.